Supplementary Material

Gated Nanoprobe Utilizing Metal–Organic Frameworks for Identifying and Distinguishing Between the Wild Strains and the Vaccine Strains of Brucella

Dong Li[a], Shuna Ren[a], Xiaotong Wang[a], Lili Chen[a], Shuang You[a], Yan Tang[b*], Lihua Chen[a*]

a Key Laboratory of Optic-electric Sensing and Analytical Chemistry for Life Science; Shandong Key Laboratory of Biochemical Analysis; Key Laboratory of Analytical Chemistry for Life Science in Universities of Shandong; Key Laboratory of Eco-chemical Engineering; College of Chemistry and Molecular Engineering, Qingdao University of Science and Technology, Qingdao 266042, PR China.

b Xinjiang Agricultural vocational Technical College; Institute of Western Agriculture, the Chinese Academy of Agricultural sciences.

*Corresponding author: Lihua Chen, E-mail: Lihuachen@qust.edu.cn, Fax: +86 53284022681; Tel: +86 15054246089. Yan Tang, E-mail: 1074086262@qq.com, Fax: +86 53284022681; Tel: +86 19915016436.

Supporting information: S1~S3, Tables S1~S4, and Figures S1~S19.

S1 Preparation of NH_2-MIL-53 (Al)

NH_2-MIL-53 (Al) was synthesized by the solvothermal method [1]. First, $AlCl_3 \cdot H_2O$ (1.52 g), NH_2-BDC (1.12 g), deionized water (15 mL), and DMF (45 mL) were added into a 100 mL stainless steel reaction kettle with a Teflon lining together, then placed in a laboratory oven at 150 °C for 24 hours. Next, after vacuum filtration, a light milky yellow product was obtained, subsequently dissolved in DMF, and refluxed at 150 °C for 8 hours. Finally, after washing with acetone and drying by vacuum, a purified NH_2-MIL-53(Al) was successfully prepared, then placed in a refrigerator at 4 °C for further use. If it is for long-term storage, the product will be placed in a vial filled with nitrogen and then placed in a dryer after the activation step. The purification step: the product was purified in boiling DMF for 5 hours to remove the remaining water molecules or unreacted ligands trapped in the pores. The activation step: the product was washed with acetone and dried in a vacuum oven at 30 °C before further analysis.

S2 Gel electrophoresis assay

First, 40% acrylamide/bisacrylamide gel solution (3.5 mL), H_2O (4.25 mL), 50 × TAE buffer (160 μL), 10% ammonium persulfate (APS) (80 μL) and TEMED (4 μL) were mixed and added into the gel plate. After 30 minutes, the freshly prepared gel was soaked in 1× TAE buffer.

Then, 10 μL each of T1, T2, WB1, WB2, T1T2, and WB1WB2 (at a concentration of 1×10^{-5} M) were individually immersed into MOF@Flu@P1h and MOF@Rho 6G@P2h (1 mL, 1:1) and incubated for 0.5 hours at 37 ℃. Subsequently, 10 μL supernatant from each mixture was collected, then thoroughly mixed with 2 μL of buffer, one by one. Subsequently, these samples were added to each lane and the power supply was activated. Finally, the gel was removed and stained with ethidine bromide (EB) solution (30 μL, diluted with deionized water) in darkness for 30 minutes. The gel was then imaged using a bioelectrophoretic image analysis system.

S3 The formula involved in manuscript

ΔFluorescence intensity in all mauscript refers to the measured fluorescence signal intensity of the sample after subtracting the non-specific fluorescence signals originating from the environment or background. (Figure 1～5 in Manuscript, S1,S2, S5, S7 in Supplementary Materials)

Nomalized ΔFluorescence intensity in Supplementary Materials refers to the measured fluorescence signal intensity of the sample after subtracting the non-specific fluorescence signals originating from the environment or background.The maximum value was set to 1.（Figure S9, S11～ S15, S17～ S19 in Supplementary Materials)

Supporting Figures

Table S1 Traditional Testing based on different substrates

Substrates	Causes of defects	Result
Antibodies and antigens[2,3,4]	Law of antibodies formation	Long periodicity
	Individual differences	False negative
Genes[5,6]	Complex primer design	False positive
	Potential genetic mutations	False negative

law of antibodies： In natural infections, IgG is frequently found in abundance, while IgM is relatively rare. Typically, IgG concentration reaches a relatively high level after one month and often persists for up to one year. Interestingly, in the immune body, IgM is more abundant than IgG, emerging as the first antibody. Furthermore, after around one week, IgM concentration becomes detectable in the bloodstream. However, its presence is temporary, typically lasting only a few weeks or months.

Individual differences: As we known, the virb12 protein or NH antibody is absent in the immune body. However, due to individual differences, the concentration of NH antibody and virb12 protein in some natural infections also keep in a low level, which will make a confused result for the subseqentely detection.

Complex primer design： The specificity of the PCR method is highly dependent on the design of the primers. However, achieving specificity can be challenging when dealing with wild strains or vaccine strains that share similar nucleic acid sequences. This raises the risk of cross-reactivity, where the PCR primers may interact with non-

target sequences, resulting in the amplification of non-specific PCR products and the potential for false-positive results. Additionally, wild strains and vaccine strains often undergo genetic mutations, which can impede successful amplification or lead to false-negative results if the PCR primers do not align with the specific regions of the target sequence where mutations occur. Hence, it is crucial to give meticulous attention to primer design in order to overcome these challenges.

Potential genetic mutations: These vaccines are produced by subjecting virulent strains to a series of passages through high temperatures, radiation, or chemical reagents, which result in a high genetic similarity between the two strains involved in this process. Similarly, wild viruses and vaccines may also display genetic mutations.

80 **Table S2** Sequences of the oligonucleotides used in this study

Name	Sequences (5'~3')
P1h	**stem-loop structure** **P1** **stem-loop structure** CCCCCCTCGCCAAGCGACTGGCCGCCAAAAGACTGCGGGGGG
P2h	**stem-loop structure** **stem-loop structure** AAAAAAATGGGTGTCGGCCCTCAATAGCGTCCCGCATTTTTT **P2**
T1	GCAGTCTTTTGGCGGCCAGTCGCTTGGCGA **Complementary to P1**
T2	TGCGGGACGCTATTGAGGGCCGACACCCAT **Complementary to P2**
T1M	GCAGCCTTTTGGCGACCAGTCGCCTGGCGA
T2M	TGCGAGACGCTATTTAGGGCCGATACCCAT
WB1	ACTAATTTCACCAGCAAGAACTCCACCTTG
WB2	CTGGGAGGGAGGACAAGGTGGAGTTCTTG
MO	ACTAATTTCACCAGCAAGAACTCCACCTTG
TB	TCGGGGTTGACCCACAAGCGCCGACTGTCGGCGCTG
Y3 (T1T2)	**Complementary to P1** **Complementary to P2** GCAGTCTTTTGGCGGCCAGTCGCTTGGCGATGCGGGACGCTATTGA **T1** **T2** GGGCCGACACCCAT
A19 (T1WB2)	**Complementary to P1** **Noncomplementary to P2** GCAGTCTTTTGGCGGCCAGTCGCTTGGCGACTGGGAGGGAGGACAA **T1** GGTGGAGTTCTTG
ZHU 1	**Complementary to P1** GCAGTCTTTTGGCGGCCAGTCGCTTGGCGATGCGAGACGCTATTTA **T1** GGGCCGATACCCAT
Others (WB1WB2)	ACTAATTTCACCAGCAAGAACTCCACCTTGCTGGGAGGGAGGACAA GGTGGAGTTCTTG

81 ***T1T2(Y3):** T1T2 refers to a lengthy sequence comprising of two shorter chain

82 sequences, namely T1T2.

T1 and T2: T1 and T2 represents two shorter chain sequences.

T1WB2(A19): T1WB2 denotes a long sequence consisting of T1 and WB2 as its constituent short chain sequences, namely T1WB2.

WB1WB2: WB1WB2 signifies a prolonged sequence made up of WB1 and WB2 as the respective short chain sequences, namely WB1WB2.

WB1 and WB2: WB1 and WB2 implies the presence of WB1 and WB2.

As shown in Table S2. The blue part is the stem-loop structure sequence of the probe and the black part is the complementary sequence of the target. The red parts are the mismatched bases.

Table S3 Gibbs free energy of the P1h, P2h, P1ss, P2ss, P1ss with T1, the P2ss with T2, the P1h with T1 and the P2h with T2.

Name	P1h	P2h	P1ss	P2ss	P1ss with T1	P2ss with T2	P1h with T1	P2h with T2
ΔG(kcal/mol)	-8.69	-5.50	0.00	0.00	-47.81	-46.81	-48.24	-47.54

The theoretical energetics: After designing the DNA strands, equilibrium probability maps and secondary structure prediction maps for P1ss with T1 (10 μM), P2ss with T2 (10 μM), P1h with T1 (10 μM), and P2h with T2 (10 μM) were generated using the NUPACK software. The Gibbs free energies of P1h and P2h were calculated to be -8.69 kcal/mol and -5.50 kcal/mol, respectively in Figure S3. These values indicate that the hairpin structures have lower energy and a more stable configuration compared to P1ss and P2ss, thus confirming their propensity to form hairpin structures. As depicted in Figure S2, the Gibbs free energies of P1h with T1 and P2h with T2 were determined to be -48.24 kcal/mol and -47.54 kcal/mol, respectively. This suggests that the probes with hairpin structures are more effective in target recognition compared to probes with a linear configuration (Table S3).

105 **Table S4** Comparison of Different Detection Methods of wild strains and vaccine
106 strains.

Method	Pathogen isolation [7,8]	ELISA [9,10]	PCR [11]	This work
Detection Principle	Bacteriology test	Immunological testing	Molecular biology testing	Genetic testing
One-step detection	NO	NO	NO	YES
Safety	Low	High	High	High
Laboratory	More than BSL-2	---	---	---
Technical personnel requirements	High	Low	High	Low
Experimental period	1~2 weeks	5 days	2~4 hours	0.5 hours
Instrument costs	Low	High	High	Low
Experimental cost	Low	Low	High	Low
Linear range	0.1~10^3 μg/ml	10-100 copies/mL	10^3~10^6 copies/mL	10^{-6}~ 10^{-9} M

107

Figure S1 the specific excitation and emission wavelengths for Flu (A) and Rho6G (B).

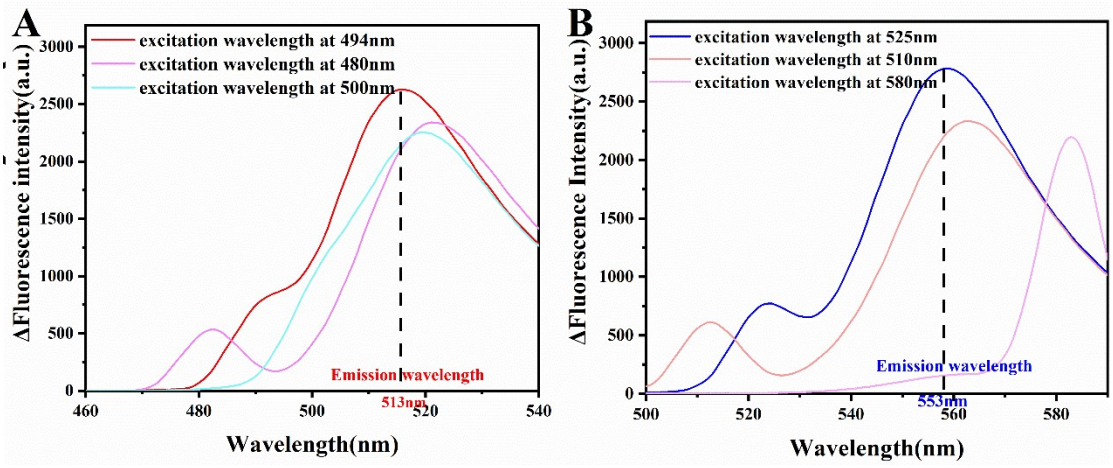

A series of excitation wavelength (480nm, 494nm, 500nm and 510nm, 525nm, 580nm) was used to get emission wavelength. As shown in Figure S1, Flu is excited at 494 nm (The excitation wavelength) and detected at 513 nm (the emission wavelength), while Rho 6G fluorescence is excited at 525 nm (The excitation wavelength) and detected at 553 nm (the emission wavelength).

Figure S2 (A) Fluorescence response of Flu in buffer. (B) Fluorescence response of Rho 6G in buffer. Fluorescence response of the mixture of Flu and Rho 6G in buffer (C) or in serum (100%) (D).

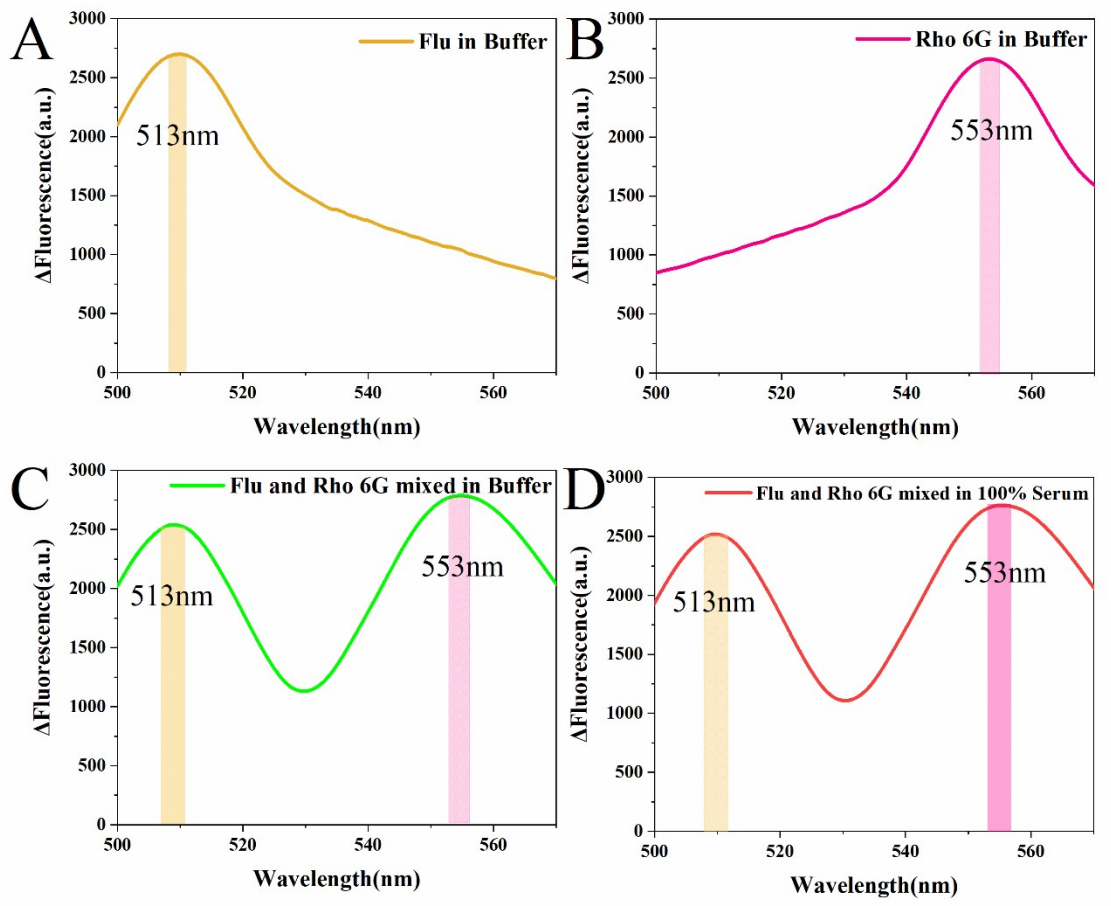

Figure S3 The structural equilibrium probability maps of P1ss and P2ss (A), P1h and P2h (B), P1ss withT1, P2ss with T2 (C), P1h with T1 and P2h with T2 (D).

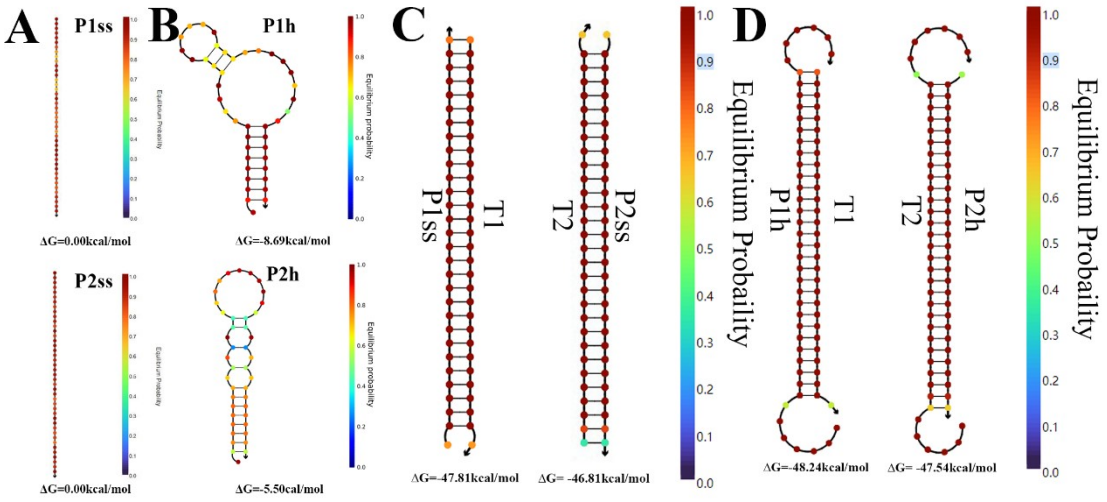

Figure S4 Mechanism (A) and PAGE (B) of Exo I-catalyzed hydrolysis for the P1ss, P2ss, P1h and P2h.

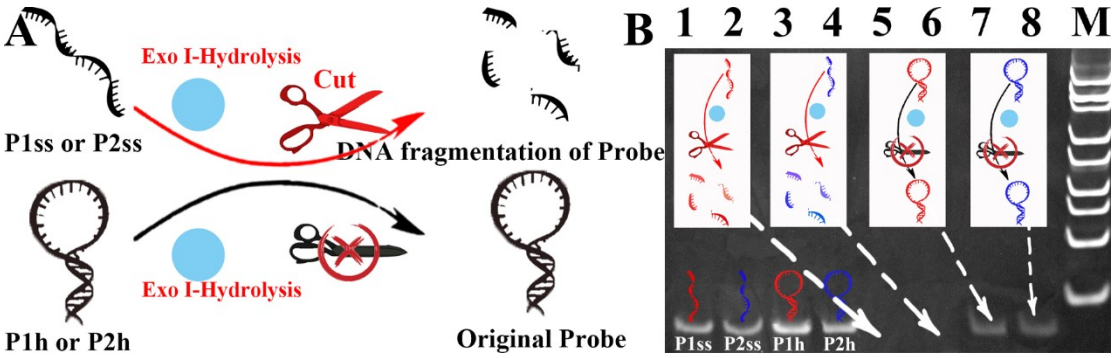

Mechanism: It has been demonstrated that Exonuclease I (Exo I), derived from E. coli, exhibits the ability to catalyze the hydrolysis of single-stranded DNA (ssDNA) specifically from its 3'-terminus, while not affecting double-stranded DNA (dsDNA). Therefore, if the hydrolysis of the single-stranded probe by Exo I is inhibited, it would serve as evidence to confirm the formation of hairpin structures by the probes shown in Figure S4A.

Experimental Procedure: Firstly, 2.0 μL of P1ss, P2ss, P1h, and P2h (10-5 M) were respectively mixed with 18 μL of Exo I (1.25 U/μL) at 37 ℃ for 0.5 hours. Subsequently, 10 μL supernatant from each mixture was collected and thoroughly mixed with 2 μL of buffer, one by one. These samples were then added to each lane and the power supply was activated. Finally, the gel was removed and stained with ethidine bromide (EB) solution (30 μL, diluted with deionized water) in darkness for 30 minutes. The gel was then imaged using a bioelectrophoretic image analysis system.

Results and Discussion: The Figure S4B show that clear bands can be observed in lanes 1, 2, 3, and 4, which correspond to P1ss, P2ss, P1h, and P2h, respectively. Lanes 5 to 8 represent the results of Exo I-catalyzed hydrolysis (30 min, 37 °C) of mixtures containing the same concentrations of P1ss, P2ss, P1h, and P2h. In lanes 7 and 8, the probe bands are still visible, indicating that the hairpin structure of the probes remains

145 intact. However, in lanes 5 and 6, the probe bands disappear, suggesting the cleavage
146 of the probe strands by Exo I. Overall, these results confirm that P1h and P2h do indeed
147 form the hairpin structure.

Figure S5 Fluorescence response for P1ss, P2ss, P1h and P2h modified with FAM and BHQ1.

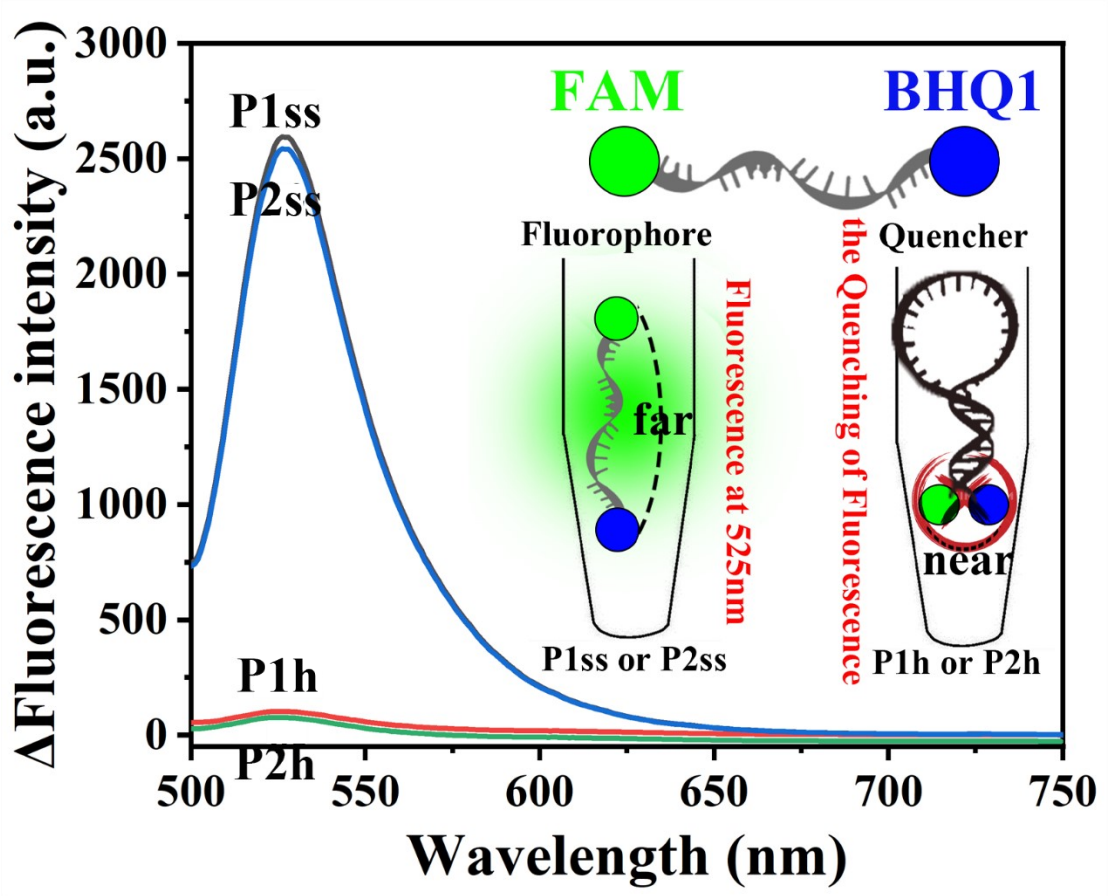

Mechanism: P1ss, P2ss, P1h and P2h were modified with FAM (the fluorescent dye) and BHQ1 (the quenching agent) markers at their ends. For P1ss and P2ss, they are the linear conformation, leading to a significant distance between FAM and BHQ1. Therefore, a strong fluorescence signal was observed. For P1h and P2h, they are the hairpin structure, so FAM and BHQ1 were forced to be close to each other. As a result, fluorescence quenching was observed.

Experimental Procedure: P1h and P2h were centrifuged at a speed of 4000 for 1 minute, then diluted into buffer. Subsequently, they were heated at 95° C for 5 minutes, then cool to room temperature. Finally, the fluorescence signal was recorded. For P1ss and P2ss, the fluorescence signal was directly measured without the other treatments.

Results and Discussion: For P1ss and P2ss, due to their linear conformation where both FAM and BHQ1 are at ends, the strong fluorescence signals were observed. Interestingly, after annealing, the hairpin structure was formed for P1h and P2h. In this case, FAM and BHQ1 were forced to be close to each other. As a result, fluorescence quenching was observed in Figure S5.

Figure S6 SEM image (A), TEM image (B), XRD (C), FTIR (D), and EDS (E) of NH_2-MIL-53 (Al).

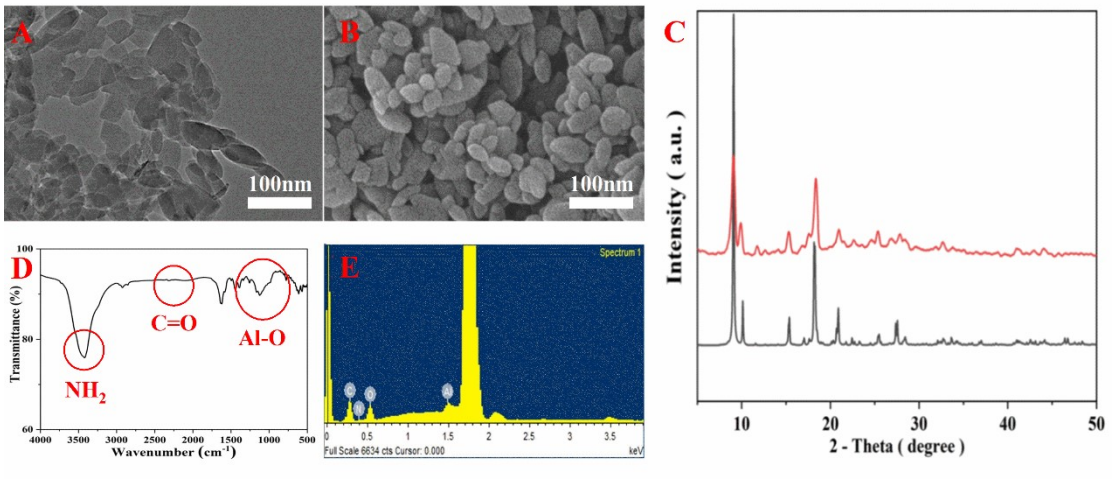

To confirm the successful synthesis of NH_2-MIL-53 (Al), a series of characterizations were carried out. Firstly, the morphology of the composite was characterized by scanning electron microscope and transmission electron microscope. It can be seen from Figure S6A that the synthesized MOF material is rhombic with an average particle size of about 100 nm. This conclusion is consistent with that reported in the literature. In addition, the corresponding TEM (Figure S6B) further proves this view. To further confirm the successful preparation of MOF, X-ray diffraction (XRD), fourier transform infrared spectroscopy (FTIR), and energy dispersive spectroscopy (EDS) were performed. The black curve and the red curve represent the XRD patterns of simulated patterns of NH_2-MIL-53 (Al) (CCDC901254) and NH_2-MIL-53 (Al). It can be seen from Figure S6C that the peak values at 2θ of 9.2°, 18.2°, 25.4°, and 27.8° are consistent with the simulation results, this indicates that MOF was successfully synthesized.

As shown in Figure S6D, the absorption peaks at 3417 cm^{-1} and 3500 cm^{-1} are related to the symmetric and asymmetric stretching of amino groups. The absorption peak at 1400-1600 cm^{-1} corresponds to the symmetric and asymmetric stretching of carbonyl groups. The Al-O vibration peak is at ~1100 cm^{-1}, 900 cm^{-1}, and 610 cm^{-1}. Additionally, elements of C, N, O, and Al were displayed in Energy dispersive spectroscopy (EDS) (Figure S6E). All these indicate that NH_2-MIL-53 (Al) has been successfully synthesized.

Figure S7 Fluorescence response of Flu, MOF@Flu, MOF@Flu@P1h, Flu@P1h, Flu@T1, Flu@P1h@T1, and MOF@Flu@P1h+T1.

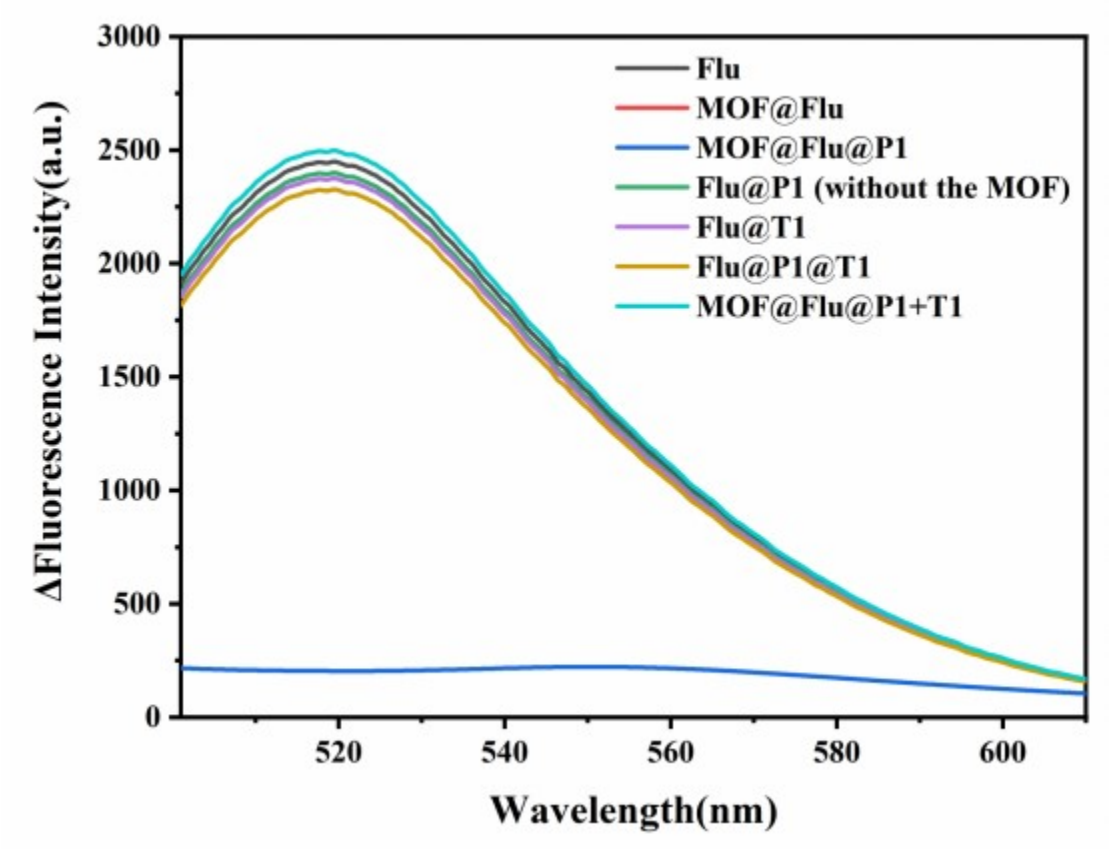

In order to assess the significance of MOFs, various samples including Flu, MOF@Flu, MOF@Flu@P1h, Flu@P1h, Flu@T1, Flu@P1h@T1, and MOF@Flu@P1h+T1 were utilized. Figure S7 illustrates the results. In the absence of MOF, the response of Flu remains unchanged and at a high level before and after the addition of the target. Conversely, the presence of MOF and P1h leads to a significant difference in the response of Flu before and after the target is added. The principal function of MOF is its notable loading capability, selective adsorption of guest molecules, and impeding interference from heteromolecules in the environment. On the other hand, the primary function of the probes is their impressive gatekeeping behavior.

Figure S8 Schematic diagram of the preparation process of MOF@Flu@P1h and MOF@Rho 6G@P2h.

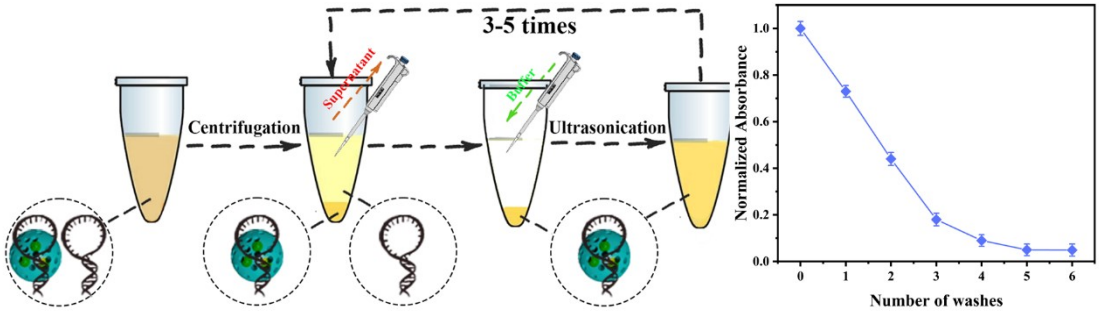

These probes, specifically DNA, initially form an ionic bond with the amino cations of the MOF through its phosphate anions, allowing the probe to be adsorbed onto the MOF surface. During the preparation of MOF@Flu@P1h and MOF@Rho 6G@P2h, water washing treatment and centrifugation were utilized multiple times. Every time, the supernatants were collected, then analyzed through UV. As shown in Figure S8, the UV absorption peak of DNA gradually decreases until reaching its lowest point. This indicated that any loosely-bonded probes from the MOF@Flu@P1h and MOF@Rho 6G@P2h and the free-style probe have been removed. Under this condition, the centrifuged product demonstrate the UV absorbance peaks at 260 and 360, indicating the successful preparation of MOF@Flu@P1h and MOF@Rho 6G@P2h (Figure 2A c, d).

Figure S9 The stability of the probe DNA on the MOF carrier. "Vibration, Centrifugation, and Ultrasonication": Fluorescent signal of Flu and Rho 6G for the supernatant collected from MOF@Flu@P1h and MOF@Rho 6G@P2h treated through the various operation, including vibration, centrifugation, and ultrasonication. Control sample: Fluorescent signal of Flu and Rho 6G for the supernatant after the introduction of T1 and T2 into MOF@Flu@P1h and MOF@Rho 6G@P2h (this fluorescent signal was set as 1). The error bars represent the standard deviation of the three samples.

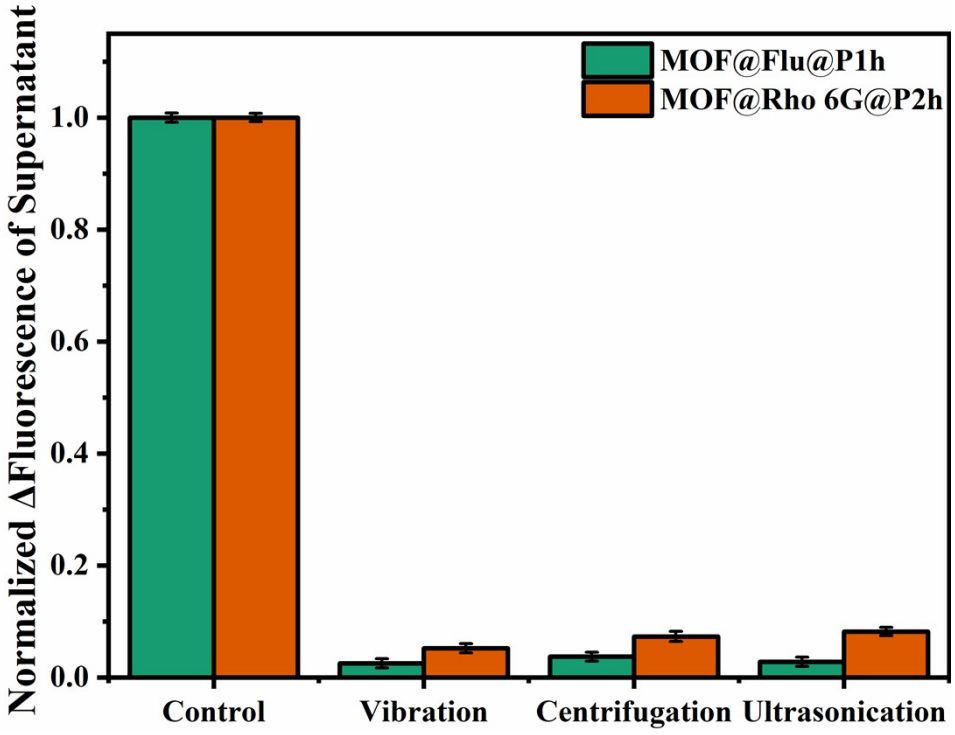

Stability: Next, the stability of probe DNA on the MOF carrier was investigated. Here, MOF@Flu@P1h and MOF@Rho 6G@P2h were soaked, shocked, centrifuged and sonicated for up to 30 min. Then the Flu and Rho 6G was detected through the collection of supernatants after the various operation. As shown Figure S9. no obvious trace of Flu and Rho 6G was found (The sample treated through vibration, centrifugation, and ultrasonication). Interestingly, the introduction of T1 and T2 can immediately trigger the door of MOF@Flu@P1h and MOF@Rho 6G@P2h (Control

232 sample). A larger number of Flu and Rho 6G rushed out from the cavity of MOF (Its
233 fluorescent signal was set as 1). This indicates that the stability of probe DNA on the
234 MOF carrier was excellent.

Figure S10 Competitive processes of MOF@Flu@P1h and MOF@Rho 6G@P2h, respectively, in the presence of the target

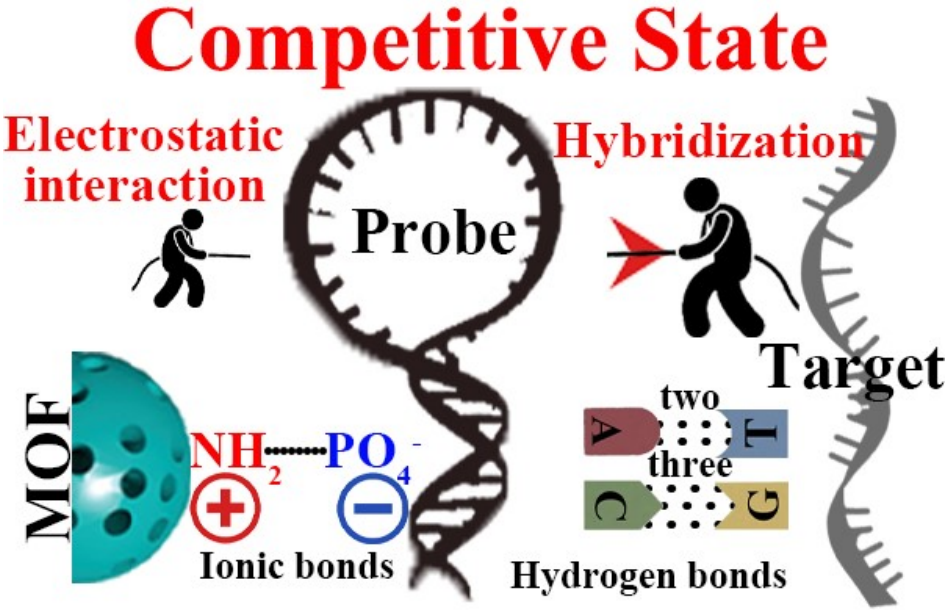

Mechanism: In the hybridization-induced platform, the probe DNA forms an ionic bond with the amino cations of MOF through its phosphate anions, facilitating the probe's adsorption onto the MOF surface. When the target substance is introduced, the hybridization between the target and the probe weakens the interactions between the probe and the MOF, resulting in the dissociation of the probe from the MOF. As a result, the fluorescent molecule is released, fulfilling the purpose of detection (Figure S10).

Figure S11 Effect of pH on the modification of MOF@Flu and MOF@Rho 6G with P1h (A) or P2h (B). Effect of pH on the hybridization between MOF@Flu@P1h and MOF@Rho 6G@P2h with T1 (C) or T2 (D). Error bars were derived from three parallel experiments.

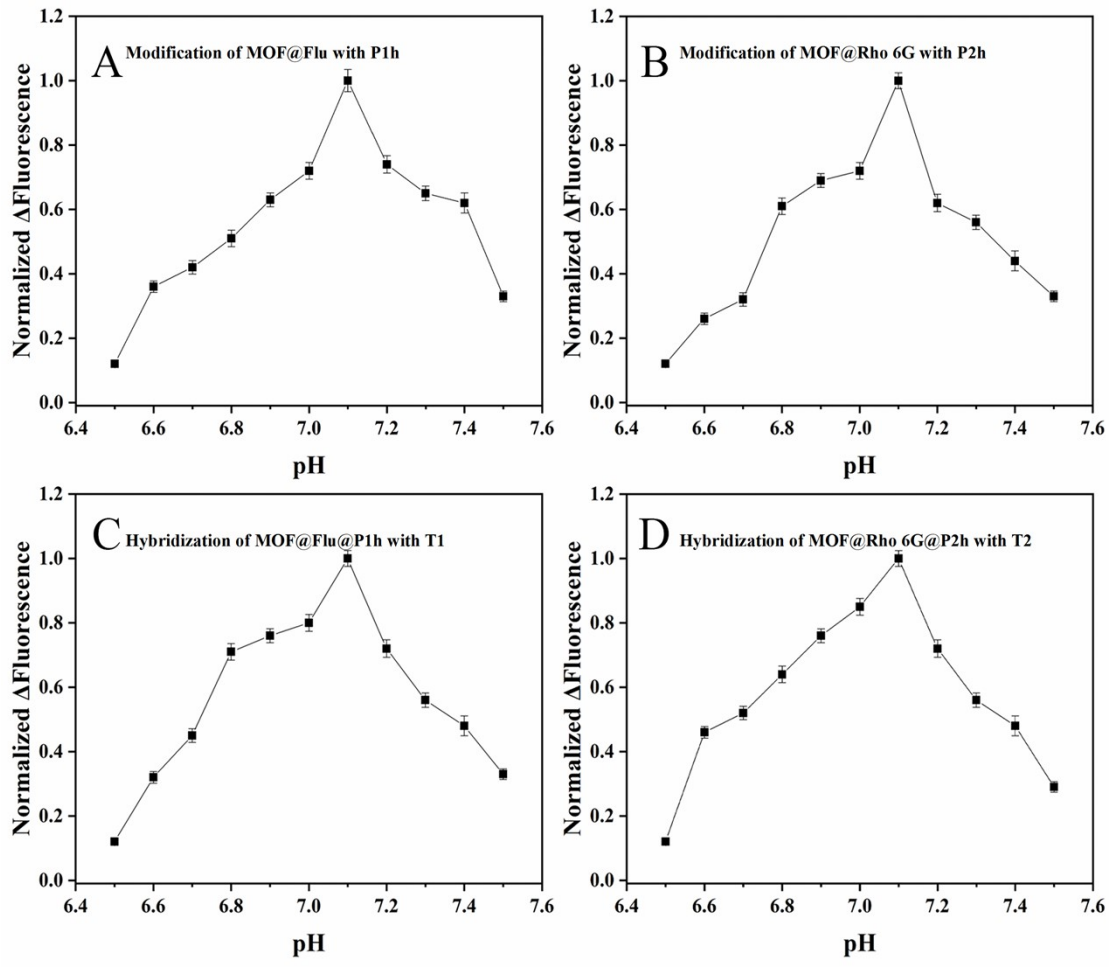

pH optimization of modification: In this experimental setup, the MOF@Flu is prepared by adding 1 mL of MOF (1 mg/mL) into 1 mL of a Flu (10 mg/mL) prepared with sodium acetate buffer (NaAc-Hac) at pH levels ranging from 6.5 to 7.5. After incubating the mixture for 12 hours at 37 ℃, P1h (10 μL, 10^{-5} M) is combined with the MOF@Flu and allowed to incubate for an additional 12 hours. This results in the formation of MOF@Flu@P1h, which is then washed with deionized water to remove any unbound P1h molecules. In a similar manner, the MOF@Rho 6G@P2h complex is

prepared by substituting Flu and P1h with Rho 6G and P2h. The MOF@Flu@P1h complex and MOF@Rho 6G@P2h complex were mixed in a 1:1 ratio with deionized water. T1T2 (10 μL, 10^{-5} M) were added to the MOF@Flu@P1h and MOF@Rho 6G@P2h (1:1, 2 mL, 1 mg/mL) solutions and incubated for 30 minutes. After centrifugation, the supernatant was collected and the relative change in fluorescence intensity (Δfluorescence intensity) was recorded.

pH optimization of hybridization: In this experimental setup, the MOF@Flu is prepared by adding 1 mL of MOF (1 mg/mL) into 1 mL of a Flu (10 mg/mL) prepared with sodium acetate buffer (NaAc-Hac) at pH 7.1. After incubating the mixture for 12 hours at 37 ℃, P1h (10 μL, 10^{-5} M) is combined with the MOF@Flu and allowed to incubate for an additional 12 hours. This results in the formation of MOF@Flu@P1h, which is then washed with deionized water to remove any unbound P1h molecules. To study the interaction between the complexes and the compound T1T2 (10 μL, 10^{-5}M) are separately added to the MOF@Flu@P1h and MOF@Rho 6G@P2h complexes. The mixture of MOF@Flu@P1h and MOF@Rho 6G@P2h (in a 1:1 ratio) is dissolved in a 2 mL buffer solution (1 mg/mL) and then incubated with the same concentrations (10 μL, 10^{-5}M) of T1T2 for 30 minutes at pH levels ranging from 6.5 to 7.5. Following incubation, the mixture is subjected to centrifugation, and the supernatant is collected. The relative change in fluorescence intensity (Δfluorescence intensity) is recorded as a measure of the interaction between the complexes and T1T2.

Here, the optimal pH values for the modification of MOF@Flu or MOF@Rho 6G with P1h (A) or P2h (B), and the hybridization between MOF@Flu@P1h and MOF@Rho 6G@P2h with T1 (C) or T2 (D), were investigated. We found that the highest fluorescence signals were observed at pH=7.1 (Figure S11).

Figure S12 Effect of temperatures on the modification of MOF@Flu and MOF@Rho 6G with P1h (A) or P2h (B). Effect of temperatures on the hybridization between MOF@Flu@P1h and MOF@Rho 6G@P2h with T1 (C) or T2 (D). Error bars were derived from three parallel experiments. The error bars represent the standard deviation of the three samples.

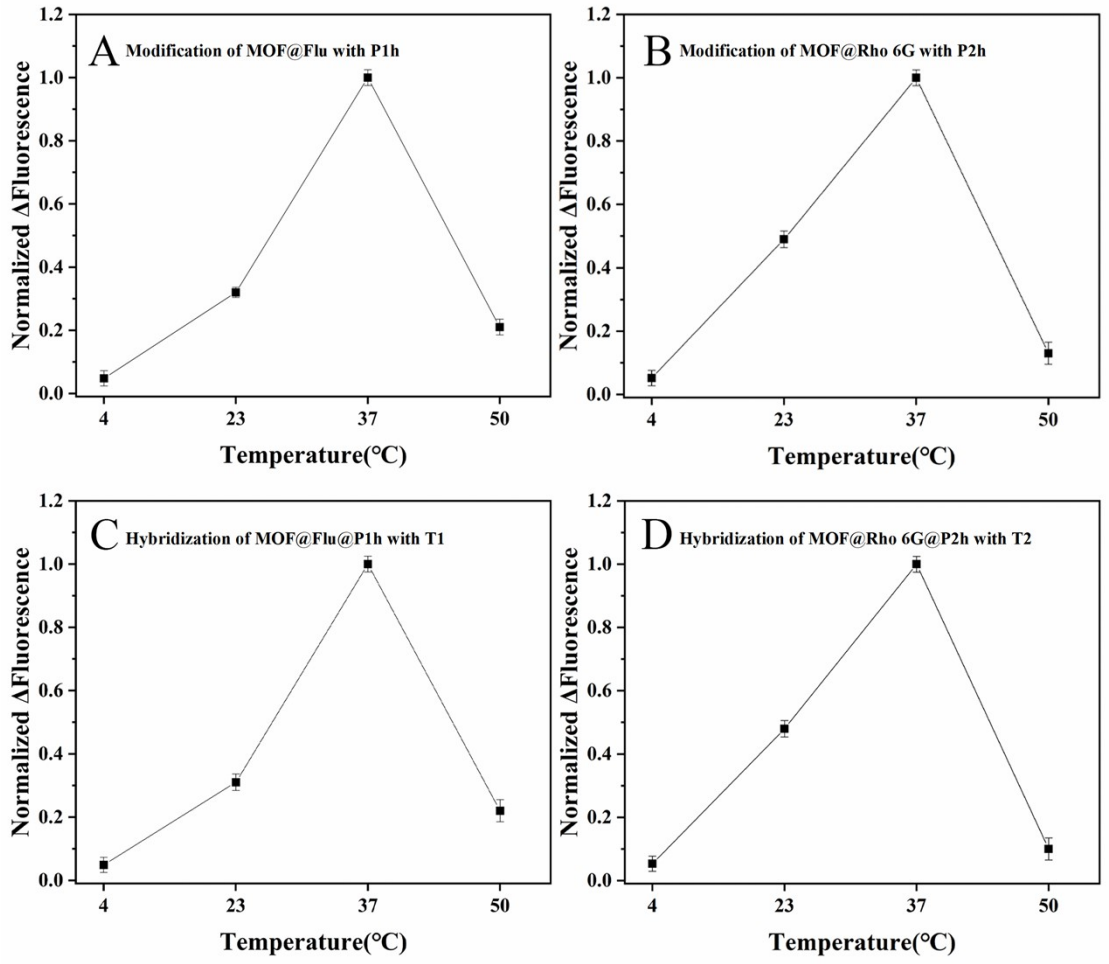

Modification temperature optimization: MOF (1 mL, 1 mg/mL) was added to the Flu (1 mL, 10 mg/mL) prepared with optimized pH and incubated for 12 hours of different reaction temperatures (4 ℃, 25 ℃, 37 ℃, 55 ℃). Subsequently, the hairpin structure P1h (10 μL, 10^{-5} M) was mixed with the MOF@Flu, and each sample was reacted for 12 hours. The loosely bound P1h (MOF@Flu@P1h) was then removed using deionized water. The same procedure was repeated to prepare the MOF@Rho

6G@P2h complex, with Rho 6G and P2h replacing Flu and P1h (MOF@Rho 6G@P2h). The MOF@Flu@P1h complex and MOF@Rho 6G@P2h complex were mixed in a 1:1 ratio with deionized water. T1T2 (10 μL, 10-5 M) were added to the MOF@Flu@P1h and MOF@Rho 6G@P2h (1:1, 2 mL, 1 mg/mL) solutions and incubated for 30 minutes. After centrifugation, the supernatant was collected and the relative change in fluorescence intensity (Δfluorescence intensity) was recorded.

Hybridization temperature optimization: In this experimental setup, the MOF@Flu is prepared by adding 1 mL of MOF (1 mg/mL) into 1 mL of a Flu (10 mg/mL) prepared with sodium acetate buffer (NaAc-Hac) at pH 7.1. After incubating the mixture for 12 hours at 37 ℃, P1h (10 μL, 10^{-5} M) is combined with the MOF@Flu and allowed to incubate for an additional 12 hours. This results in the formation of MOF@Flu@P1h, which is then washed with deionized water to remove any unbound P1h molecules.The MOF@Flu@P1h complex and MOF@Rho 6G@P2h complex were mixed in a 1:1 ratio with deionized water. T1T2 (10 μL, 10-5 M) were added to the MOF@Flu@P1h and MOF@Rho 6G@P2h (1:1, 2 mL, 1 mg/mL) solutions and incubated for 30 minutes. After centrifugation, the supernatant was collected and the relative change in fluorescence intensity (Δfluorescence intensity) was recorded. An experiment was carried out to investigate the effect of different reaction temperatures (4 ℃, 25 ℃, 37 ℃, 55 ℃) on the fluorescence signal, while keeping other conditions constant.

4 ℃, 23 ℃, 37 ℃, and 50 ℃ were utilized to optimize the temperature conditions for the modification of MOF@Flu and MOF@Rho 6G using P1h (A) or P2h (B) and the subsequent hybridization between MOF@Flu@P1h and MOF@Rho 6G@P2h with T1 (C) or T2 (D). As depicted in Figure S12A and Figure S12B, it was observed that 37 ℃ represents the optimal temperature for both the modification of

MOF@Flu and MOF@Rho 6G with P1h (A) or P2h (B) and the hybridization between MOF@Flu@P1h and MOF@Rho 6G@P2h with T1 (C) or T2 (D).

Figure S13 Effect of time on the modification of MOF@Flu and MOF@Rho 6G with P1h (A) or P2h (B). Error bars were derived from three parallel experiments. The error bars represent the standard deviation of the three samples.

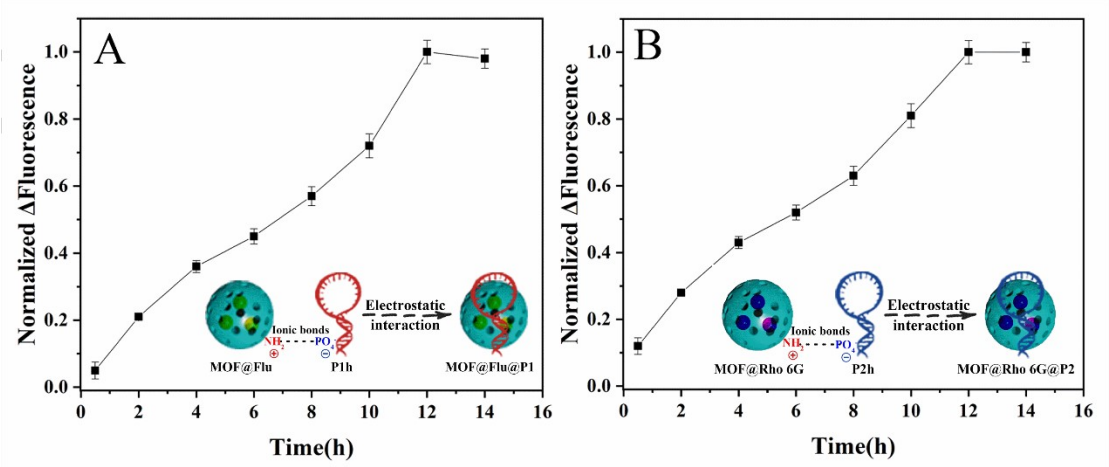

Optimization of modification time: The MOF solution (1 mL, 1 mg/mL) was added to the Flu solution (1 mL, 10 mg/mL) at the optimized pH and incubated for 12 hours. Then, the hairpin structure P1h (10 μL, 10-5 M) was mixed with the MOF@Flu solution, and each sample was allowed to react for various time points including 0 h, 2 h, 4 h, 6 h, 8 h, 10 h, 12 h, 14 h, and 16 h. Finally, the loosely bound P1h (MOF@Flu@P1h) complex was removed using deionized water. The same procedure was repeated for the preparation of MOF@Rho 6G@P2h, except that Rho 6G and P2h were used instead of Flu and P1h (MOF@Rho 6G@P2h). The MOF@Flu@P1h complex and the MOF@Rho 6G@P2h complex were mixed in a 1:1 ratio with deionized water. T1T2 (10 μL, 10-5 M) were added to the MOF@Flu@P1h and MOF@Rho 6G@P2h (1:1, 2 mL, 1 mg/mL) solutions and incubated for 30 minutes. After centrifugation, the supernatant was collected, and the relative change in fluorescence intensity (Δfluorescence intensity) was recorded.

Firstly, several MOF@Flu@P1h and MOF@Rho 6G@P2h were prepared through incubation between MOF@Flu or MOF@Rho 6G and P1h or P2h at different time (0

h, 2 h, 4 h, 6 h, 8 h, 10 h, 12 h, 14 h, and 16 h). The fluorescence signal strength of the supernatant was then detected after the respective addition of T1 or T2 to the several MOF@Flu@P1h or MOF@Rho 6G@P2h. As shown in Figure S13, the optimal incubation time was determined to be 12 h.

Figure S14 Fluorescence response of MOF@Flu@P1h and MOF@Rho 6G@P2h to the addition of T1T2 in several possible coexisting interfering substances, including metal ions (K^+, Na^+), proteins (BSA, BP26 DA) (A)and complex biological systems (1%,5%,10%,20% and 30% serum) (B). The error bars represent the standard deviation of the three samples.

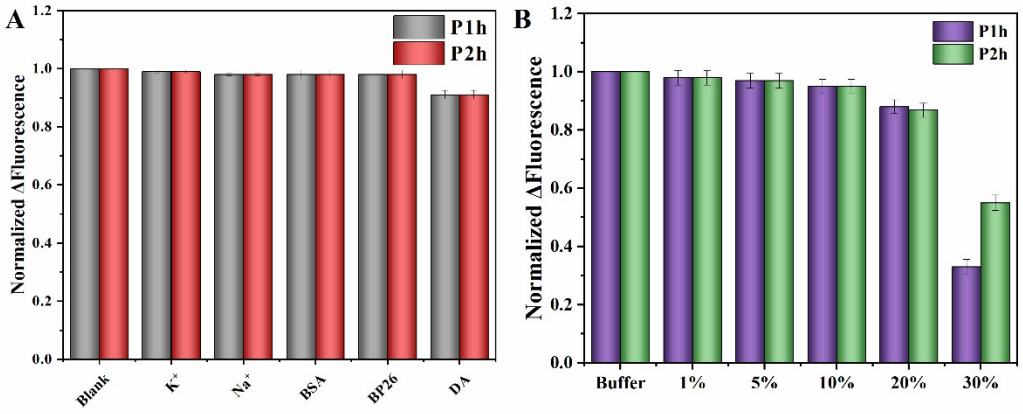

As depicted in the Figure S14, MOF@Flu@P1h and MOF@Rho 6G@P2h demonstrated negligible interference from various substances, including up to 20% serum, signifying their robustness and reliability in detecting target DNA sequences in real samples.

Figure S15 Assessment of detection capability from numerous tests for MOF@Flu@P1h (A) and MOF@Rho 6G@P2h (B). The x axis was an arbitrary laboratory number and was omitted for clarity.

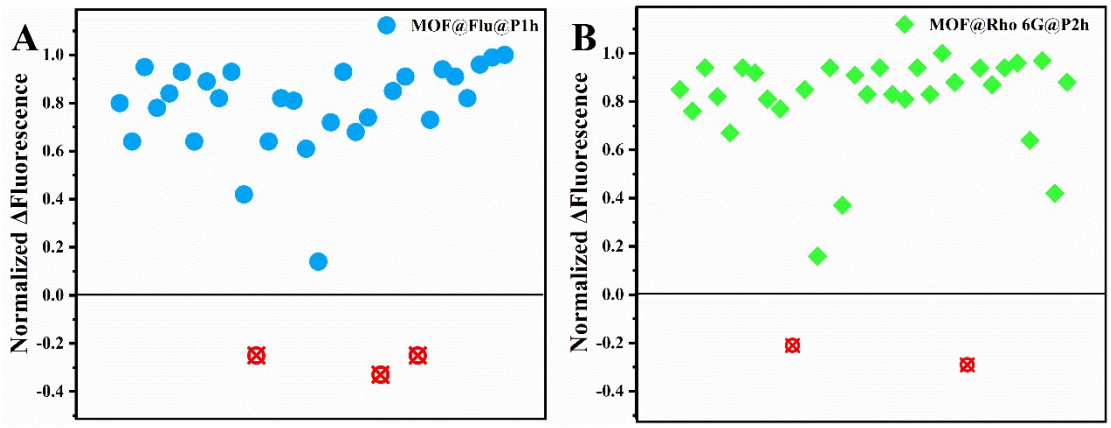

Figure S16 Comparison of prices with commercial products.

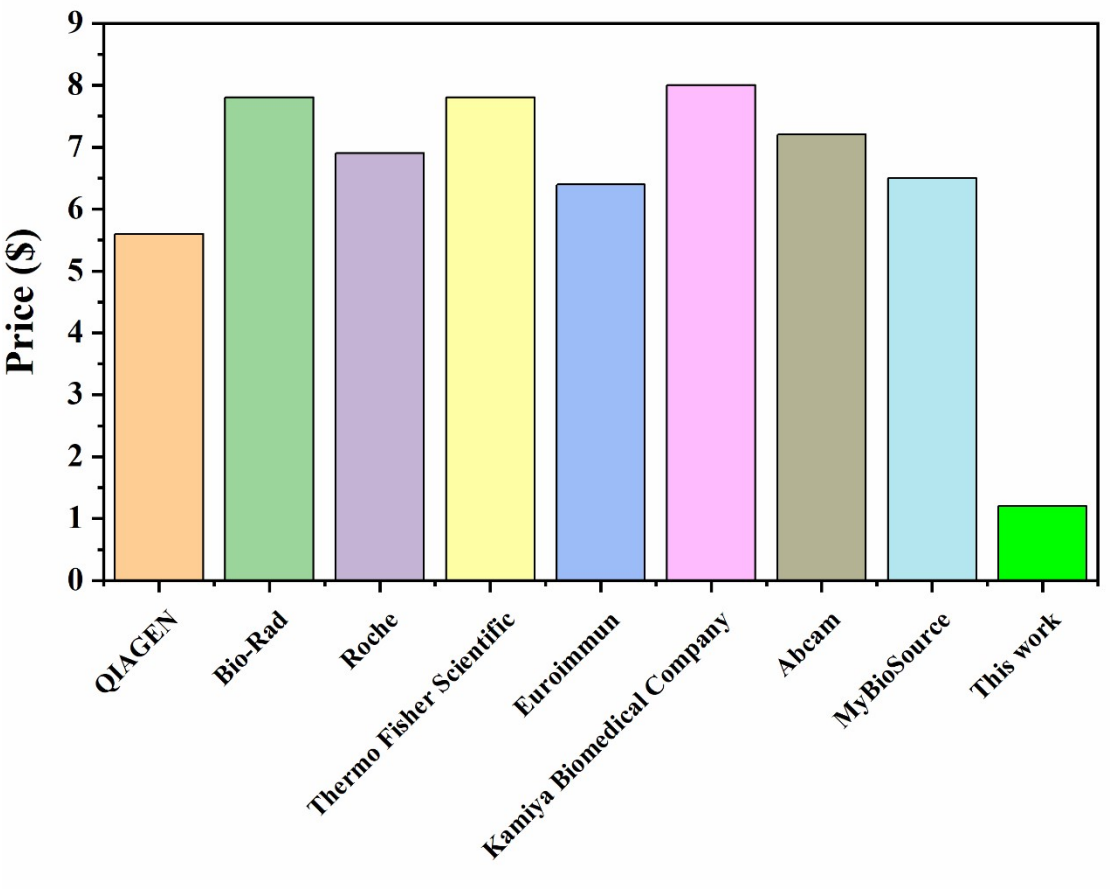

Currently, in Figure S16 commercially available products such as QIAGEN, Bio-Rad, Roche, Thermo Fisher Scientific PCR kits, and Euroimmun, Kamiya Biomedical Company, Abcam, MyBioSource ELISA kits are priced at around $8 in Figure S16. Our strategy primarily relies on MOFs, dyes, probes, and testing costs. According to their market price, for each detection, approximately $0.27 should be paied for probes, $0.77 for MOF, $0.019 for Flu and $0.027 for Rho 6G. So, $1 was determined in our strategy. Additionally, the raw materials for MOF@Flu@P1h and MOF@Rho 6G@P2h can be regenerated, and even after five cycles of recycling, the detection efficiency remains as high as 90%. This provides significant benefits in terms of

368 reducing the price of our strategy. Although this differs from the calculation of
369 commercial product prices, a low cost can be still considered.

Figure S17 The impact of different storage conditions (pH, buffer and temperature) on the performance of MOF@Flu@P1h and MOF@Rho 6G@P2h. (A) After being stored at different pH for 3 days, the detection performance of MOF@Flu@P1h and MOF@Rho 6G@P2h after adding T1T2 (a), T1WB2 (b) and WB1WB2 (c). (B) Storage time of MOF@Flu@P1h (a) and MOF@Rho 6G@P2h (b) at different temperatures. (C) After being stored at different buffer for 3 days, the detection performance of MOF@Flu@P1h and MOF@Rho 6G@P2h after adding T1T2 (a), T1WB2 (b) and WB1WB2 (c). The error bars represent the standard deviation of the three samples.

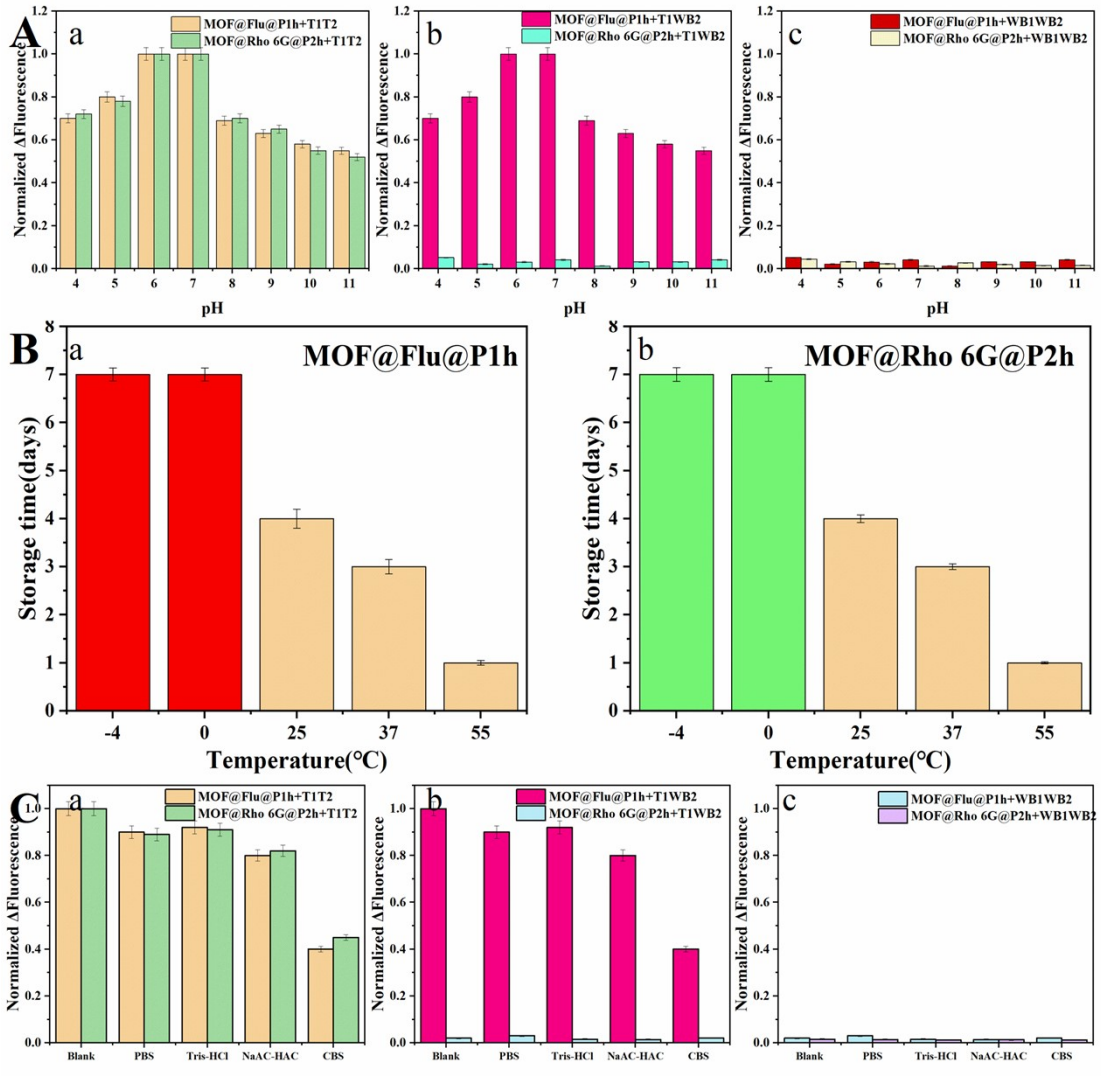

The fluorescence signal of MOF@Flu@P1h and MOF@Rho 6G@P2h remained relatively stable for the optimal duration within the pH range of 6 to 7 after 3 days (Figure S17A) between -4 °C to 0 °C **(**Figure S17B**)** in the different buffering solutions (Figure S17C**)**.

Figure S18 Fluorescence response of MOF@Flu@P1h and MOF@Rho 6G@P2h under the addition of T1T2 (A), T1WB2 (B), and WB1WB2 (C) at different time intervals (Blank,1 day,2 days,3 days,4 days,7 days). Error bars were derived from three parallel experiments. The error bars represent the standard deviation of the three samples.

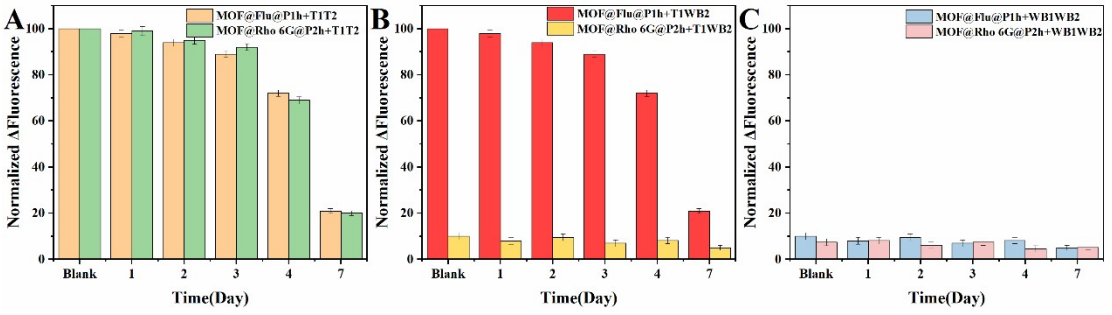

We investigated the stability of MOF@Flu@P1h and MOF@Rho 6G@P2h by testing their detection performance at different time intervals. As depicted in Figure S18, the probe's detection efficiency reduced gradually as the duration of storage increased. After a 2 days interval, the fluorescence signal exhibited only a 5% change, which increased to 10% after 3 days, 30% after 4 days, and nearly 80% after 7 days. These results highlight that the optimal time to utilize MOF@Flu@P1h and MOF@Rho 6G@P2h is within 7 days after their preparation.

Figure S19 Fluorescence response of the regenerated MOF@Flu@P1h and MOF@Rho 6G@P2h under the addition of T1T2 at different cycle times (1, 2, 3, 4, 5, 6). Error bars were derived from three parallel experiments. The error bars represent the standard deviation of the three samples.

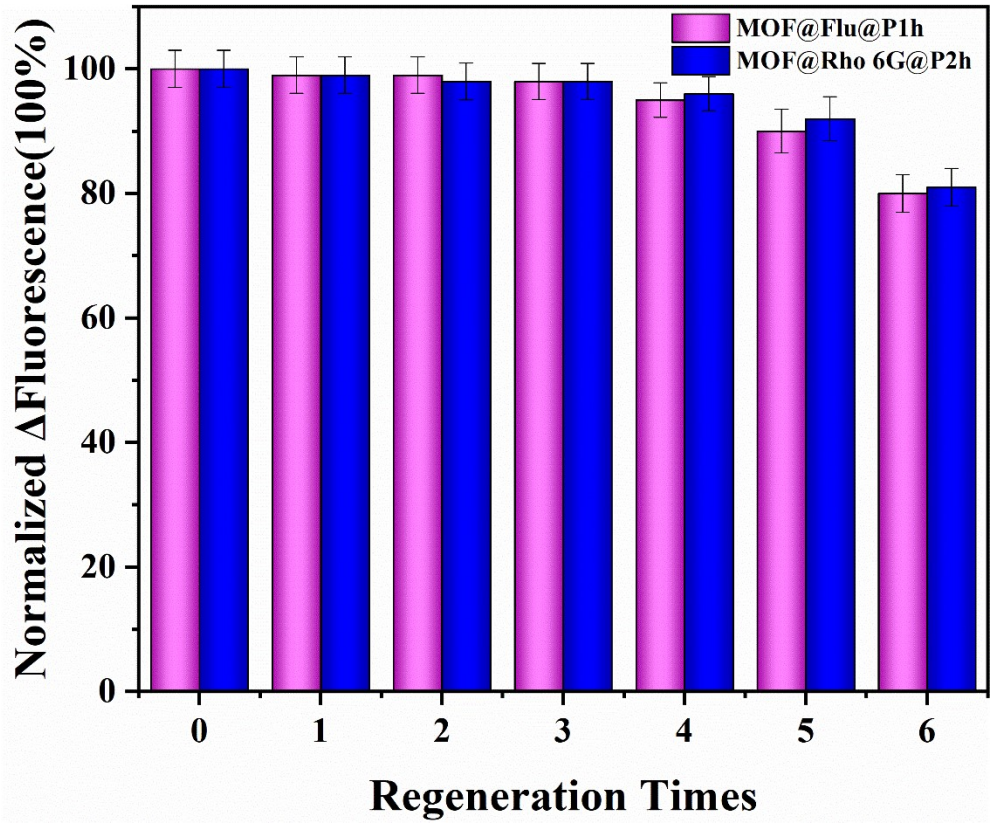

In this procedure, we aim to regenerate MOF@Flu@P1h and MOF@Rho 6G@P2h, which has been used, through a high concentration of urea (10M). Subsequently, we will perform new sensing modifications and detection processes. Based on our experimental findings, the sensitivity of the sensing decreases significantly after replenishing five times (Figure S19).

References

1. X. Cheng, A. Zhang, K. Hou, M. Liu, Y. Wang, C. Song, G. Zhang, Size-and morphology-controlled NH_2-MIL-53 (Al) prepared in DMF–water mixed solvents，*Dalton Transactions*, 2013, **42**, 13698-13705. https://doi.org/10.1039/C3DT51322J

2. A. Cavaglià, N. Gromov, J. Julius, Bootstrability in defect CFT: integrated correlators and sharper bounds, *Journal of High Energy Physics*, 2022, **2022**, 1-59. https://doi.org/10.1007/JHEP05(2022)164

3. D. Averaimo, F. De Massis, G. Savini, G. Garofolo, F. Sacchini, A. Abass, M. Tittarelli, G. Migliorati, Detection of Brucella abortus Vaccine Strains RB51 in Water Buffalo (Bubalus bubalis) Milk, *Pathogens*, 2022, **11**, 748. https://doi.org/10.3390/pathogens11070748

4. A. Das, B. Kumar, S. Chakravarti, K. P. Singh, Single-tube duplex-PCR for specific detection and differentiation of Brucella abortus S19 vaccine strains from other Brucella spp, *Indian Journal of Animal Research*, 2019, **53**, 821-826. https://doi.org/10.18805/ijar.

5. B-3584 Bányász B, Antal J, Dénes B, False Positives in Brucellosis Serology: Wrong Bait and Wrong Pond, *Tropical Medicine and Infectious Disease*, 2023, **8**, 274. https://doi.org/10.3390/tropicalmed8050274

6. Y. Lin, C. Cao, W. Shi, C. Huang, S. Zeng, J. Sun, J. Wu, Development of a triplex real-time PCR assay for detection and differentiation of gene-deleted and wild-type African swine fever virus, *Journal of Virological Methods*, 2020, **280**,

113875. https://doi.org/10.1016/j.jviromet.2020.113875

7. A. Bulashev, O. Akibekov, Z. Suranshiyev, B. Ingirbay, A. Sciences, Serodiagnostic potential of Brucella outer membrane and periplasmic proteins，*Turkish Journal of Veterinary & Animal Sciences*, 2019, **43**, 486-493. https://doi.org/10.3906/vet-1902-75

8. A. Khan, A. Sayour, F. Melzer, S. El-Soally, M. Elschner, W. Shell, A. Moawad, S. Mohamed, A. Hendam and U. Roesler, Seroprevalence and molecular identification of Brucella spp. in camels in Egypt, *Microorganisms*, 2020, **8**, 1035. https://doi.org/10.3390/microorganisms8071035

9. M. Tabasi, S. Eybpoosh, S. Bouzari, Development of an indirect ELISA based on whole cell Brucella abortus S99 lysates for detection of IgM anti-Brucella antibodies in human serum, *Comparative immunology, microbiology and infectious diseases*, 2019, **63**, 87-93. https://doi.org/10.1016/j.cimid.2019.01.007

10. R. Hans, P. K. Yadav, P. K. Sharma, M. Boopathi and D. Thavaselvam, Development and validation of immunoassay for whole cell detection of Brucella abortus and Brucella melitensis *Scientific reports*, 2020, **10**, 8543. https://doi.org/10.1038/s41598-020-65347-9

11. L. Che, C. Qi, W. Bao, X. Ji, J. Liu, N. Du, L. Gao, K. Zhang and Y. Li, Monitoring the course of Brucella infection with qPCR-based detection *International Journal of Infectious Diseases*, 2019, **89**, 66-71. https://doi.org/10.1016/j.ijid.2019.09.013